Low clouds suppress Arctic air formation and amplify high-latitude continental winter warming

Timothy W. Cronin[a,1] and Eli Tziperman[a,b]

[a]Department of Earth and Planetary Sciences, Harvard University, Cambridge, MA 02138; and [b]School of Engineering and Applied Sciences, Harvard University, Cambridge, MA 02138

Edited by Isaac M. Held, Geophysical Fluid Dynamics Laboratory, National Oceanic and Atmospheric Administration, Princeton, NJ, and approved July 31, 2015 (received for review June 3, 2015)

High-latitude continents have warmed much more rapidly in recent decades than the rest of the globe, especially in winter, and the maintenance of warm, frost-free conditions in continental interiors in winter has been a long-standing problem of past equable climates. We use an idealized single-column atmospheric model across a range of conditions to study the polar night process of air mass transformation from high-latitude maritime air, with a prescribed initial temperature profile, to much colder high-latitude continental air. We find that a low-cloud feedback—consisting of a robust increase in the duration of optically thick liquid clouds with warming of the initial state—slows radiative cooling of the surface and amplifies continental warming. This low-cloud feedback increases the continental surface air temperature by roughly two degrees for each degree increase of the initial maritime surface air temperature, effectively suppressing Arctic air formation. The time it takes for the surface air temperature to drop below freezing increases nonlinearly to ∼10 d for initial maritime surface air temperatures of 20 °C. These results, supplemented by an analysis of Coupled Model Intercomparison Project phase 5 climate model runs that shows large increases in cloud water path and surface cloud longwave forcing in warmer climates, suggest that the "lapse rate feedback" in simulations of anthropogenic climate change may be related to the influence of low clouds on the stratification of the lower troposphere. The results also indicate that optically thick stratus cloud decks could help to maintain frost-free winter continental interiors in equable climates.

global warming | polar amplification | cloud feedbacks | paleoclimate

One of the persistent mysteries of the "equable climates" of the Eocene and Cretaceous, ∼ 143–33 million years ago, is the warmth of midlatitude and high-latitude continental interiors during winter and, in particular, the frost-intolerant flora and fauna in parts of what is now Wyoming and southern Canada (1). Climate models can simulate warm conditions over the ocean, but they have difficulty simulating continental warmth away from the moderating effects of the ocean, especially if tropical warming is constrained to be $\lesssim 10$ °C. Although recent work suggests a relaxation of such tropical constraints (2), model−data agreement has been found only for model CO_2 concentrations that seem unrealistically high, and the mechanisms that maintain high-latitude warmth over land remain poorly understood (2, 3). Previous proposed mechanisms to explain the overall reduction of the equator−pole temperature contrast in equable climates include polar stratospheric clouds (4, 5), dramatic expansion of the Hadley circulation (6), increased poleward ocean heat transport due to ocean mixing by stronger tropical cyclones (7, 8), and a convective cloud feedback (9). The convective cloud feedback has now appeared in multiple simulations of past and future climates at high CO_2 (10, 11) but is not effective at explaining warmth over land; the other possible mechanisms remain speculative at this point.

Mechanisms that underlie high-latitude continental warmth in past equable climates are also potentially relevant to understanding current and future climate change. The Arctic and high-latitude land in North America and Asia have warmed much more rapidly than the global mean temperature in recent decades (12, 13). Furthermore, climate models predict a significant future amplification of winter warming over the Arctic, both land and ocean (14–16). Numerous mechanisms have been proposed to explain Arctic amplification (15), including ice albedo feedbacks (17), meridional structure in the Planck feedback (18), increased moist static energy transport by the atmosphere (19), a convective cloud feedback (9), and changes in the stability of the atmosphere, with stronger warming near the surface (20). Such surface-amplified warming—also referred to as a positive "lapse rate feedback"—leads to a smaller increase in outgoing longwave radiation than would occur for the same amount of warming spread over the depth of the troposphere, because much of the emission from the lower troposphere is absorbed before reaching the top of the atmosphere. Recent analysis across a set of climate models suggests that the lapse rate feedback is the strongest contributor to the enhanced high-latitude warming (16).

Unfortunately, our understanding of why warming is surface-amplified at high latitudes is relatively poor. The high-latitude lapse rate feedback is merely a diagnostic measure, which identifies enhanced warming as a consequence of the a priori unknown vertical structure of that warming. The vertical temperature structure of the Arctic atmosphere may change due to many mechanisms, including changes in sea ice area, clouds, water vapor, or atmospheric heat transport (21). This differs from the simpler case of the tropics, where constraints imposed by moist convection allow for a direct prediction of the lapse rate and how it changes with climate (16).

The goal of this paper is to suggest that both the high-latitude lapse rate feedback and winter continental warmth in equable climates may be tied to the process of very cold continental air mass formation during winter. It has been shown that lower-tropospheric

Significance

Future-greenhouse simulations, and evidence of frost-intolerant species in high-latitude continental interiors during past equable climates, show significantly amplified warming at high latitudes over land in winter, with physical mechanisms that are still not understood. We show that the process of Arctic air formation, in which a high-latitude maritime air mass is advected over a continent, cooled at the surface, and transformed into a much colder continental polar air mass, may change dramatically and even be suppressed in warmer climates due to an increase in the duration of optically thick low clouds. This leads to two-degree warming over the continent in response to each degree of warming over the nearby ocean, possibly explaining both past and future continental warming.

Author contributions: T.W.C. and E.T. designed research, performed research, analyzed data, and wrote the paper.

The authors declare no conflict of interest.

This article is a PNAS Direct Submission.

[1]To whom correspondence should be addressed. Email: timothywcronin@fas.harvard.edu.

This article contains supporting information online at www.pnas.org/lookup/suppl/doi:10.1073/pnas.1510937112/-/DCSupplemental.

mixed-phase clouds play a critical role in the formation of Arctic air (22). We show that Arctic air formation may be suppressed in warmer climates, leading to significant continental warming during winter. Specifically, we perform simulations with a single-column model of an air mass that begins over the ocean and is advected over high-latitude land. We find that increased lifetime of low-level liquid clouds with warming of the initial atmospheric state leads to a slower surface cooling rate and to a less stably stratified lower troposphere, consistent with the lapse rate feedback in climate models. We also analyze Coupled Model Intercomparison Project phase 5 (CMIP5) climate model results and show that aspects of Arctic amplification in such models are consistent with the proposed mechanism.

Results

We follow previous studies that took a Lagrangian perspective, using single-column models, to gain insight into how a column of air moves from high-latitude open ocean, or from lower latitudes, into a region of the Arctic during polar night, is cooled at the surface, and is transformed into polar continental air (22–26). We prescribe the initial vertical temperature and humidity profiles of an atmospheric air column, and allow it to evolve for 2 wk in the absence of solar heating and over a very low heat capacity surface representing land, snow, or sea ice. To robustly explore the role of clouds, we use several different cloud microphysical parameterizations. Further details of the model setup are provided in *Materials and Methods*.

Fig. 1*A* shows the cooling of the atmosphere for a reference simulation with the initial 2-m atmospheric temperature $T_2(0) =$ 0 °C, corresponding to present-day high-latitude ocean surface conditions. Snapshots of the vertical profile of temperature and clouds are shown every 2 d over a 14-d period. Cooling and condensation near the surface lead to formation of an optically thick mixed-phase cloud layer within the first day, which largely has dissipated by day 2 (green-blue line near 950 hPa). Subsequent cooling leads to a much deeper but optically thin ice cloud layer by day 6 (thinner blue lines), which persists for the rest of the 2-wk period, slightly slowing surface cooling but not preventing development of a strong surface-based inversion. Purple lines in Fig. 1*C* show the evolution of both the 2-m and 850-hPa air temperature; for most of the 2-wk period, after the mixed-phase cloud layer dissipates, the atmosphere is warmer at 850 hPa than at the surface, by 10–15 °C. This simulation illustrates the key features of Arctic air formation in the present-day climate (22, 26). As explained by ref. 22, the clouds in this situation do little to reduce the cooling of the surface itself, and also facilitate the direct cooling of the lower troposphere to space.

The process of surface cooling is qualitatively different for a warmer initial state, with $T_2(0) = 20$ °C (motivated by past equable climates). Initial cooling leads to a thick liquid fog and stratus cloud layer that forms by day 2, moves upward to 800 hPa by day 6, and persists until the last 2 d of the simulation (Fig. 1*B*). The surface air temperature does not fall below freezing until day 9 (orange solid line in Fig. 1*C*), and falls below the 850-hPa temperature only by a few degrees at the end of the simulation. Although the warm initial state has higher stability, its stability after 2 wk of cooling is much lower than that of the reference simulation, and a surface-based inversion develops only toward the end of the simulation. These changes in lower-tropospheric lapse rate with warming are consistent with the high-latitude lapse-rate feedback diagnosed in global models, which is an important contributor to polar amplification (16). The final surface air temperature in the warm simulation is ∼ 40 °C warmer than in the reference simulation despite an initial surface warming of only 20 °C relative to the reference simulation (Fig. 1*C*). These dramatic results amount to a suppression of Arctic air formation in a much warmer climate.

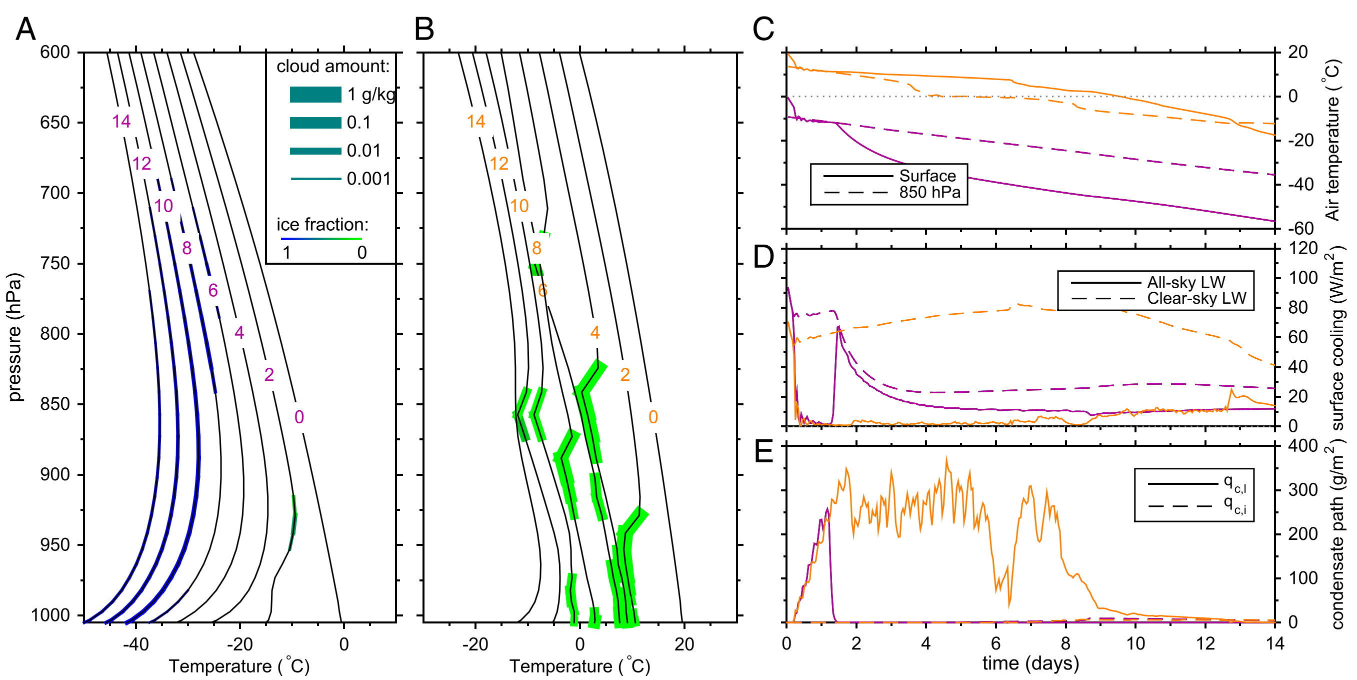

Fig. 1. Single-column simulation results of polar air formation for cold and warm initial atmospheric columns. A reference simulation with initial 2-m air temperature $T_2(0) = 0°$ C is shown in *A* and by purple lines in *C*–*E*. A simulation with much warmer initial 2-m air temperature $T_2(0) = 20°$ C is shown in *B* and by orange lines in *C*–*E*. In *A* and *B*, black lines show temperature profiles every 2 d as a function of pressure; solid colors overlaying the temperature profiles indicate where clouds are found, total cloud water content is indicated by line thickness, and cloud phase is indicated by color, with green being all liquid and blue being all ice. *C* shows the evolution of air temperature at 2-m height (solid) and 850 hPa (dashed), *D* shows the net longwave cooling of the surface for actual (solid) and hypothetical clear-sky (dashed) conditions, and *E* shows the evolution of vertically integrated cloud liquid ($q_{c,l}$, solid) and cloud ice ($q_{c,i}$, dashed). The Lin microphysics scheme is used for these two simulations; other microphysics schemes show qualitatively similar features.

The importance of clouds can by seen by comparing net longwave surface cooling rates with and without clouds (Fig. 1*D*). The difference between the solid and dashed purple lines, corresponding to the simulation with $T_2(0) = 0$ °C, indicates that clouds only weakly influence the surface cooling, except in the brief period between days 1 and 2 when a thick mixed-phase stratus layer forms. The difference between the solid and dashed orange lines, corresponding to the $T_2(0) = 20$ °C simulation, is larger and more persistent, indicating that clouds reduce surface cooling for nearly the entire duration of the simulation. The influence of initial temperature can also be seen in plots of the vertically integrated cloud liquid and ice amounts; the warm initial state develops and retains more liquid water in clouds (Fig. 1*E*).

The reduced rate of cooling in response to higher initial temperature $T_2(0)$ is robust with respect to the microphysics scheme used, as seen in the difference between the initial temperature and the time mean 2-m air temperature over the duration of the simulation, $\Delta T_2 = T_2(0) - \overline{T_2}$ (Fig. 2*A*). The average surface cooling across microphysics schemes for $T_2(0) = 0$ °C is $\Delta T_2 \approx 38$ °C, and is reduced by 21 °C to $\Delta T_2 \approx 17°$ C for $T_2(0) = 20°$ C. The suppression of Arctic air formation thus amplifies warming of the initial atmospheric state by over a factor of two.

The time taken for the 2-m air temperature to drop below freezing, τ_0, is less than 0.5 d if $T_2(0) < 10°$ C, but rises steeply to ∼10 d for $T_2(0) = 20°$ C (Fig. 2*B*). This nonlinearity is a consequence of the differential surface cooling rates under clear and cloudy skies as well as the use of a threshold-crossing metric; the surface initially cools rapidly under clear skies, but cools much more slowly once clouds form, with a temperature plateau for many days (solid orange line in Fig. 1*C*). Thus, for $T_2(0) < 10°$ C, the surface drops below freezing before clouds form and τ_0 is relatively insensitive to $T_2(0)$, but for $T_2(0) > 10°$ C, the surface drops below freezing after clouds form, and τ_0 is much more sensitive to $T_2(0)$.

Sensitivity tests allow us to decompose the reduced rate of cooling into contributions from cloud radiative effects, latent heat release, and clear-sky longwave radiation effects. The dash-dotted line marked "no microphysics" in Fig. 2*A* indicates the cooling that takes place in simulations where no phase change of water is allowed, and thus no cloud formation or latent heat release. The modestly reduced cooling of this case at higher $T_2(0)$ owes to the decrease in clear-sky surface radiative cooling with higher atmospheric temperature (see also Fig. 1*D*, comparing initial surface longwave cooling rates). The dash-dotted line marked "no CRF" in Fig. 2*A* shows the cooling that takes place when phase change of water is allowed, but clouds have no effect on radiative transfer calculations. The difference between the "no microphysics" and "no CRF" simulations thus indicates that the influence of latent heat release on the reduction of surface cooling is only ∼3° C at $T_2(0) = 20°$ C. The large difference between the no CRF dash-dotted line and the set of solid lines, including the black multimicrophysics mean line, shows that cloud−radiation interactions dominate the reduced cooling with warmer $T_2(0)$. Furthermore, simulations representing clouds as only liquid regardless of temperature (dash-dotted line labeled "no ice") show reduced cooling for all $T_2(0)$, and also a weaker sensitivity of ΔT_2 to $T_2(0)$. These sensitivity tests demonstrate that most of the simulated reduction in cooling arises from the radiative effects of clouds, and relates to a change in the phase of cloud particles from ice to liquid.

Consider next the role of CO_2, first by allowing its concentration to vary, with $T_2(0)$ held constant. The mean across microphysics schemes shows that each doubling of CO_2 leads to a modest 0.57–0.77 °C increase in the 2-wk average temperature, $\overline{T_2}$ (Fig. S1). Next, specifying a doubling of CO_2 along with each 4 °C increase in $T_2(0)$, we find that the fraction of warming due to clear-sky processes increases (compare "no microphysics" curves in Figs. 2*A* and S2*A*), yet the warming is similar to that obtained by only changing the initial temperature $T_2(0)$. The direct influence of changes in CO_2 is thus small compared with that of changes in clouds.

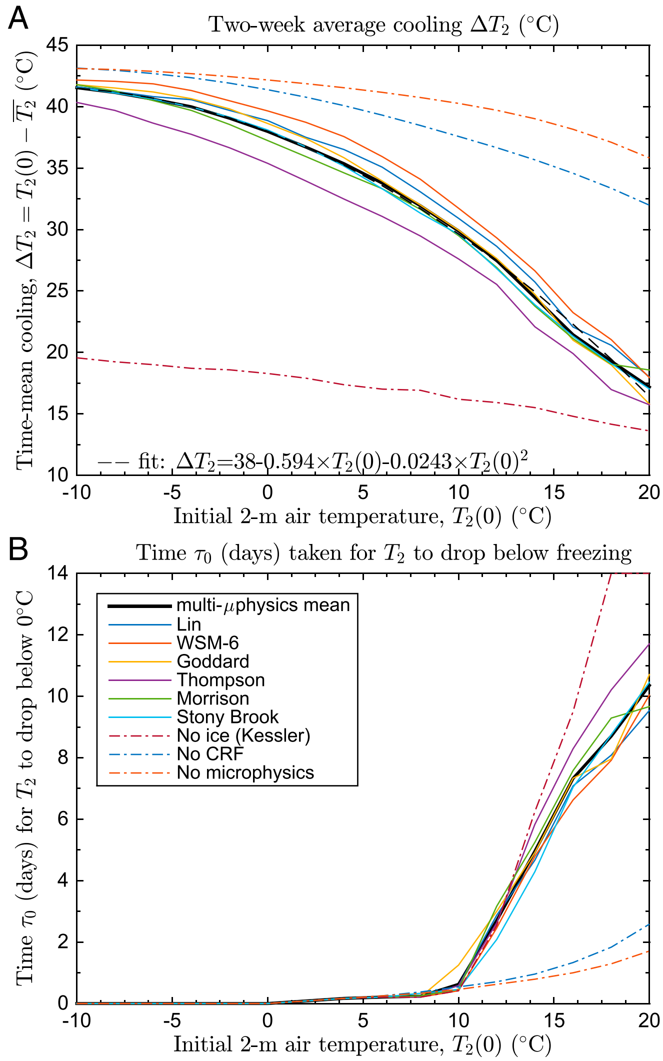

Fig. 2. Simulation results for (*A*) average surface cooling over 2-wk period, ΔT_2 (° C), and (*B*) number of days taken for the 2-m air temperature to drop below freezing, τ_0, both as a function of $T_2(0)$. Black line ("multi-µphysics mean") indicates an average across the solid-line microphysics parameterizations, which contain both liquid- and ice-phase processes. Dash-dotted lines show unrealistic microphysics assumptions used to diagnose the response mechanism; "no microphysics" indicates no phase change of water allowed, and thus no clouds at all; "no CRF" indicates that clouds are allowed to form but do not affect radiative transfer; "No ice (Kessler)" indicates a microphysics scheme that has only liquid condensate, regardless of temperature. A quadratic fit to the solid black line in *A* is shown in black dashes, with the fit shown at the bottom of *A*.

Additional sensitivity tests demonstrate robustness to the initial relative humidity profile, because the large decrease in near-surface temperature always leads to supersaturation and cloud formation at some point in the cooling process (Figs. S3 and S4). Our main results are also robust to the inclusion of subsidence, which limits the upward growth of the cloud deck for warmer initial conditions (Fig. S5) and weakens but does not eliminate the role of clouds in suppressing Arctic air formation (Fig. S6). Simulations with smaller and larger surface heat capacities (Figs. S7 and S8) show that the sensitivity of ΔT_2 to $T_2(0)$ is larger for a lower heat capacity surface, because of stronger inversions at low temperatures corresponding to the present climate.

CMIP5 (27) climate model results are consistent with our findings that climate warming leads to more low clouds over land at high latitudes during winter, which contribute to amplified warming. We compare boreal winter (DJF) multimodel mean changes between a historical period from 1980 to 1999 and a future projection for the most strongly forced Representative Concentration Pathway scenario (RCP8.5) (27) from 2080 to 2099 (models listed in *Materials and Methods*). Fig. 3 shows that maximum changes in surface air temperature, longwave cloud radiative effect on the surface energy balance, and cloud liquid condensate path occur over the Arctic Ocean and high-latitude land. The boreal winter surface cloud longwave radiative effect decreases in most regions but increases over high-latitude land and the Arctic Ocean, by an amount comparable to or greater than the forcing from increased greenhouse gas concentrations (Table 1). These large increases in liquid water content and surface longwave cloud radiative effect over the winter Arctic are consistent with suppression of Arctic air formation by low clouds in a warmer world. The findings in Fig. 3 and Table 1 extend related previous work (11, 28–32) by focusing on surface longwave cloud changes in winter, across a set of models, rather than looking at annual mean or top-of-atmosphere radiative changes, or surface changes in only a single model.

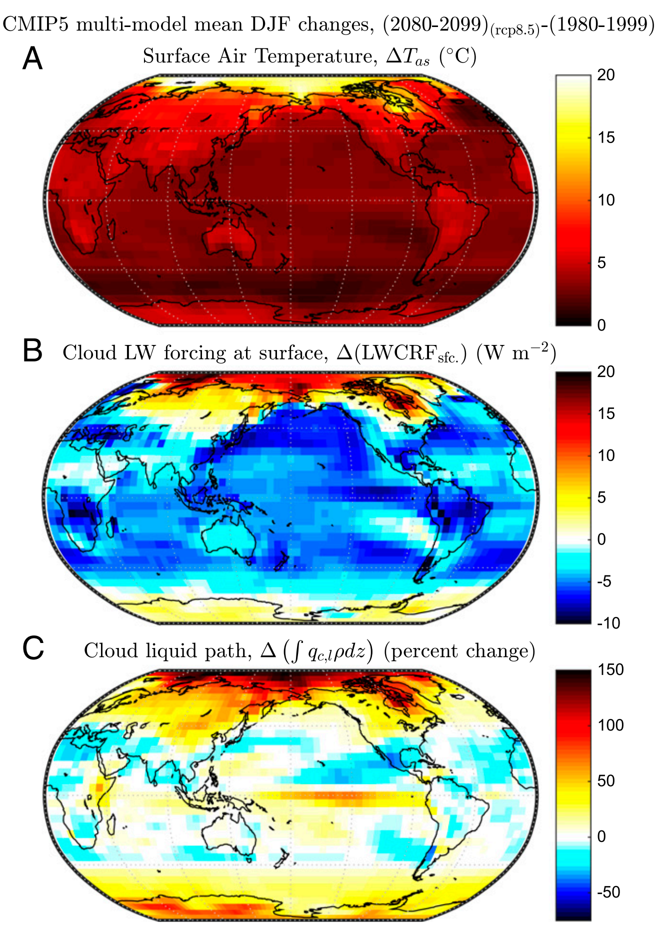

Fig. 3. Maps of mean changes in DJF variables across 11 coupled climate models, as differences between historical simulations (1980–1999) and future simulations with the RCP8.5 radiative forcing scenario (2080–2099). *A* shows changes in surface air temperature (degrees Celsius), *B* shows changes in surface longwave radiative forcing by clouds (watts per square meter), and *C* shows percentage changes in the vertical integral of cloud liquid, which more than doubles over some high-latitude regions. Note the amplified response over high-latitude continents and the Arctic.

Discussion

With regard to explaining warm continental interiors in equable climates, the time to freezing (Fig. 2*B*) can be compared with the time it takes an air mass to traverse a continent. At 5 m/s, an air parcel moves 4,320 km in 10 d, comparable to the east–west width of North America. Fig. 2*B* implies that maintaining frost-free conditions a few thousand kilometers downwind of a warm ocean, even in polar night, can be accomplished with the aid of insulation by low clouds. Thus, the long-standing problem of explaining how crocodiles and palm trees could survive winters in the Eocene in Wyoming (1), 2,000 km east of the moderating effect of the Pacific Ocean, may be resolved by our finding of suppressed Arctic air formation in warmer climates, given a sea surface temperature of $\gtrsim 15$ °C at 45°N, consistent with proxy evidence (2). Furthermore, we have assumed polar night, and thus zero insolation, but even at the winter solstice, insolation is ~ 120 $\mathrm{W{\cdot}m^{-2}}$ at 45°N, which would delay surface freezing for a longer period. Cold air outbreaks in Wyoming may result from advection of cold air from higher latitudes, but we have also shown that such higher-latitude air will likely be considerably warmer at the surface due to the role of clouds in suppressing Arctic air formation. We expect that a reduced surface cooling rate at high latitudes over land would translate into a reduction in the severity and frequency of extreme cold events at midlatitudes, consistent with observed recent changes (33).

The change from mixed-phase to liquid-phase clouds in warmer climates strongly reduces surface cooling for two reasons. First, cloud ice has less of an influence on radiative transfer per unit mass of condensate, because ice has larger particle sizes than liquid and thus less surface area per unit mass. Second, clouds have smaller residence times (time mean vertically integrated cloud condensate, divided by time mean precipitation rate) in mixed-phase and ice clouds due to both faster sedimentation of ice particles (22, 29, 34) and rapid formation of snow via the Wegener–Bergeron–Findeisen process in mixed-phase clouds (22, 34). We find that, despite a great deal of scatter, most microphysics schemes show such an increase in cloud residence time with warming (Fig. S9).

Another reason clouds may reduce cooling over high-latitude land in warmer climates is simply the increase in water vapor content, and thus net condensation, under warmer initial conditions, which will lead to more total cloud condensate even if cloud water residence time is constant. So long as cloud water residence time does not decrease sharply with warming, low-cloud condensate over land will increase with warming, leading to optically thicker clouds, a greater cloud fraction, or both. Increasing condensation with warming, rather than agreement on microphysical processes that govern cloud water residence time, is therefore the probable reason that climate models agree on increases in high-latitude low-cloud amount in winter with warming (Fig. 3) (29, 30).

Arctic cloud amount is predicted to increase with warming in both the lower and upper troposphere (9, 11, 29). Top-of-atmosphere cloud radiative changes are expected to be driven largely by changes in high clouds, whereas surface cloud radiative changes are driven largely by changes in low clouds. Our single-column model produces few upper-level clouds because the initial condition is dry in the upper troposphere. The clouds we simulate in the single-column model thus have little influence on the top-of-atmosphere energy budget, yet they still reduce surface cooling dramatically. Our examination of CMIP5 model results for high-latitude land in winter shows that changes in the cloud radiative effect are smaller by about 35–40% at the top of the atmosphere compared with the surface (Table 1), indicating an important role for low clouds, consistent with the column model results.

A seasonal rather than annual mean perspective is important when interpreting Arctic cloud changes. An annual mean cloud cooling effect at the top of the atmosphere may be a consequence of negative shortwave feedbacks in summer offsetting

Table 1. CMIP5 zonal mean and model mean changes in surface temperature and cloud radiative forcing, for DJF, showing the difference [2080–2099] minus [1980–1999]

	Land			Ocean		
Latitude band, degrees	ΔT_{as}, °C	Δ LWCRF$_{sfc.}$, W·m^{-2}	Δ LWCRF$_{TOA}$, W·m^{-2}	ΔT_{as}, °C	Δ LWCRF$_{sfc.}$, W·m^{-2}	Δ LWCRF$_{TOA}$, W·m^{-2}
60–65	9.7 (1.6)	6.6 (3.0)	5.0 (1.7)	8.3 (2.1)	2.2 (1.5)	3.3 (2.2)
65–70	11.4 (2.5)	8.3 (4.1)	5.5 (2.2)	10.7 (1.9)	4.3 (2.4)	5.5 (1.8)
70–75	12.4 (3.1)	9.2 (5.1)	5.4 (2.6)	15.5 (3.5)	10.2 (4.7)	9.0 (3.3)
75–80	11.5 (2.9)	7.6 (4.4)	4.9 (2.5)	18.4 (4.6)	14.5 (6.5)	11.0 (4.4)
80–85	—	—	—	19.7 (5.9)	16.3 (6.9)	11.3 (6.1)
85–90	—	—	—	20.3 (6.8)	16.7 (7.2)	10.9 (7.1)

Parentheses indicate SD across models.

year-round positive longwave feedbacks, and clouds in the Arctic not increasing in height as much as clouds in other places, reducing top-of-atmosphere longwave cloud effects (30). Such annual mean top-of-atmosphere analysis, however, obscures the important role of clouds in altering the winter surface temperature and lapse rate of the lower troposphere (31), and in suppressing Arctic air formation. A year-round increase in cloud fraction damps the seasonal cycle of surface temperature, via increased shortwave reflection during summer and stronger longwave heating during winter, and is therefore in line with proxy evidence of equable climates.

One limitation of this study is that our single-column model has either 0% cloud fraction or 100% cloud fraction at each level at a given time step. This suggests that future work exploring the process of Arctic air formation in a 2D or 3D high-resolution model would likely be productive. Another useful test of the low-cloud feedback proposed here would be to examine variability or trends in the observational record; data from individual stations, for example, could be used to explore whether the cooling of stagnant air masses over high-latitude land in winter is indeed weakened for warmer initial air masses. In the real world, changes in the temperature, lapse rate, and cooling rate of high-latitude air over land would also feed back on large-scale atmospheric dynamics, including the subsidence experienced during the process of cold air formation. Global climate models could be used to investigate this feedback, as well as the role of changes in atmospheric circulation with warming on the process of Arctic air formation.

An even stronger warming over land than found in our column model may be expected when accounting for additional factors not considered here, such as shorter time spent by air columns over low heat capacity surfaces due to reduced winter sea ice cover in warmer climate, increases in surface heat capacity over land due to reduced snow cover, and CO_2 increase.

Conclusions

We have analyzed the sensitivity of cold air formation using a single-column model and 3D climate model output. Using the column model, we prescribed the initial sounding of the atmosphere corresponding to an air column starting over a high-latitude open ocean, and allowed it to evolve for 2 wk in the absence of solar heating over a low heat capacity surface corresponding to high-latitude land, snow, or sea ice. We find that with warmer initial conditions corresponding to a warmer ocean, surface cooling is strongly suppressed due to the increasing lifetime and optical thickness of low clouds. These low clouds distribute the cooling over a deeper layer of the atmosphere, and thus amplify the warming at the surface relative to that aloft, which also suggests low clouds as an important potential cause of lapse-rate changes seen in simulations of future CO_2 -induced warming.

Large changes in cloud radiative effect on the surface energy budget occur in coupled climate models due to cloud phase and microphysics changes (34), temperature effects on adiabatic water content (35–37), and changes in large-scale moisture convergence and evaporation (29). Furthermore, observations of internal variability and trends indicate that a warmer Arctic will also likely be cloudier in winter (38, 39). Taken along with our proposed effects of low clouds on polar air formation and other low-cloud effects in warmer climates (32), these lines of evidence point to a robust feedback between low clouds and high-latitude winter warming. Despite having only a weak influence on top-of-atmosphere radiative balance, low clouds at high latitudes may play a key role in equable climates, as well as in current and future climate change.

Materials and Methods

We use a single-column configuration of the advanced research Weather Research and Forecasting model [WRF v3.4.1 (40)]. Key aspects of the model setup include the initial profiles of temperature and humidity, and the physics parameterizations used. The initial temperature profile has a prescribed 2-m temperature $T_2(0)$, and a lapse rate of either the moist pseudoadiabatic value or −8 K/km, whichever is more stable; the tropopause at −60 °C demarcates the base of an isothermal stratosphere. The initial humidity profile decreases from 80% at the surface (1,000 hPa) to 20% at 600 hPa, and is constant at 20% up to the tropopause; the water vapor mixing ratio is set to 5 ppm above the tropopause. The atmosphere is relaxed with a 1-d time scale to a vertically uniform eastward wind of 5 m/s. Large-scale subsidence is zero in all simulations except those shown by Figs. S5 and S6, wherein subsidence is implemented by using a vertical velocity profile $w(z) = (27/4)w_s(z/z_m)(1 - z/z_m)^2$ to advect potential temperature, water vapor, and condensed water (this profile has peak subsidence w_s at $z = z_m/3$, goes to zero at $z = 0$ and $z = z_m$, and is set to zero above $z = z_m$; we use z_m = 12 km). The vertical coordinate of the WRF model is $\eta = (p_{hs} - p)/(p_{hs} - p_{ht})$, where p is the grid cell pressure, p_{hs} is the hydrostatic surface pressure, and p_{ht} is the model-top hydrostatic pressure. We determine the position of model level i (out of $N = 51$ total) using a grid with finer spacing in the lower troposphere (11 levels are below 900 hPa); $\eta_i = 1 - [(i-1)/(N-1)]^{1.6}$. Our main results are not sensitive to the number of vertical levels used or their precise spacing, and increasing the resolution does not change them significantly, although using a lower resolution in the lower atmosphere leads to weaker surface inversions, especially for low $T_2(0)$. We use the Rapid Radiative Transfer Model (RRTMG) scheme (41) for longwave radiative transfer, with CO_2 set to 300 ppm unless otherwise noted; no shortwave scheme is needed (simulations occur during polar night). We use the Yonsei University planetary boundary layer scheme (42), and the surface is defined as a slab with a heat capacity equivalent to a water layer of 5 cm depth, independent of temperature. This choice of slab thickness is justified by considering the diffusive penetration depth into a homogeneous snow surface with volumetric heat capacity $C = 6 \times 10^5$ J·m^{-3}·K^{-1}, thermal diffusivity $D = 5 \times 10^{-7}$ m^2·s^{-1}, and a time scale $\tau = 10^5$ s ($\approx$ 1 d). The water-equivalent slab depth, z_{eff} is given by the ratio of heat capacity of the medium to that of water, times the diffusive penetration depth z^*, $z_{\mathrm{eff}} = (C/C_w)z^*$, where $z^* = \sqrt{2D\tau}$. These parameters give $z^* = 0.32$ m, and thus $z_{\mathrm{eff}} \approx 5$ cm. Note that a larger effective slab depth $z_{\mathrm{eff}} \approx 15$ cm (as in Fig. S8) would be more appropriate for a land surface without snow cover. We use the following microphysics schemes: Kessler (43), Lin (44), WSM-6 (WRF single-moment 6-class) (45), Goddard (46), Thompson (47), Morrison (48), and Stony Brook (49). Examining water and energy conservation, we diagnose a consistent ~ 3–4 W·m^{-2} spurious heat source in the column integral of dry enthalpy c_pTdp/g (approximating the dry thermodynamic equation in WRF) and a ~ 0.01 mm·d^{-1} spurious water source—but imbalances are small compared with average 2-wk tendencies, and do not show systematic dependence on temperature.

The following 11 CMIP5 models were used in this study to calculate mean changes between historical (1980–1999) and RCP8.5 (2080–2099) periods: (*i*) BCC-CSM1-1, Beijing Climate Center, China Meteorological Administration; (*ii*) CanESM2, Canadian Centre for Climate Modeling and Analysis; (*iii*) CCSM4, National Center for Atmospheric Research; (*iv*) CNRM-CM5, Centre National de Recherches Météorologiques; (*v*) GFDL-CM3, NOAA Geophysical Fluid Dynamics Laboratory; (*vi*) HadGEM2-ES, Met Office Hadley Centre; (*vii*) INMCM4, Institute for Numerical Mathematics; (*viii*) IPSL-CM5A-MR, Institut Pierre-Simon Laplace; (*ix*) MIROC5, Japan Agency for Marine-Earth Science and Technology; and (*x*) MPI-ESM-MR, Max Planck Institute for Meteorology; (*xi*) MRI-CGCM3; Meteorological Research Institute.

ACKNOWLEDGMENTS. We thank two anonymous reviewers for helpful comments and for suggesting several useful sensitivity experiments. This work was supported by a National Oceanic and Atmospheric Administration Climate and Global Change Postdoctoral Fellowship and by the Harvard University Center for the Environment (T.W.C.), and by the National Science Foundation climate dynamics program under Grant AGS-1303604. E.T. thanks the Weizmann Institute for its hospitality during parts of this work. We acknowledge the World Climate Research Programme's Working Group on Coupled Modelling, which is responsible for Coupled Model Intercomparison Project (CMIP), and we thank the climate modeling groups listed in *Materials and Methods* for producing and making available their model output. The US Department of Energy's Program for Climate Model Diagnosis and Intercomparison provides coordinating support for CMIP and led development of software infrastructure for Earth System Science Portals in partnership with the Global Organization.

1. Greenwood D, Wing S (1995) Eocene continental climates and latitudinal temperature gradients. *Geology* 23(11):1044–1048.
2. Huber M, Caballero R (2011) The early Eocene equable climate problem revisited. *Clim Past* 7(2):603–633.
3. Winguth A, Shellito C, Shields C, Winguth C (2010) Climate response at the Paleocene-Eocene thermal maximum to greenhouse gas forcing—A model study with CCSM3. *J Clim* 23(10):2562–2584.
4. Sloan LC, Walker JC, Moore TC, Jr, Rea DK, Zachos JC (1992) Possible methane-induced polar warming in the early Eocene. *Nature* 357(6376):320–322.
5. Kirk-Davidoff D, Schrag D, Anderson J (2002) On the feedback of stratospheric clouds on polar climate. *Geophys Res Lett* 29(1):L01556.
6. Farrell B (1990) Equable climate dynamics. *J Atmos Sci* 47(24):2986–2995.
7. Emanuel K (2002) A simple model of multiple climate regimes. *J Geophys Res* 107(D9): 4077.
8. Korty R, Emanuel K, Scott J (2008) Tropical cyclone-induced upper-ocean mixing and climate: Application to equable climates. *J Clim* 21(4):638–654.
9. Abbot D, Tziperman E (2008) Sea ice, high-latitude convection, and equable climates. *Geophys Res Lett* 35(3):L03702.
10. Abbot D, Walker C, Tziperman E (2009) Can a convective cloud feedback help to eliminate winter sea ice at high CO_2 concentrations? *J Clim* 22(21):5719–5731.
11. Arnold NP, et al. (2014) Effects of explicit atmospheric convection at high CO_2. *Proc Natl Acad Sci USA* 111(30):10943–10948.
12. Chylek P, Folland C, Lesins G, Dubey M, Wang M (2009) Arctic air temperature change amplification and the Atlantic Multidecadal Oscillation. *Geophys Res Lett* 36(14): L14801.
13. Hartmann D, et al. (2013) Observations: Atmosphere and surface. *Climate Change 2013: The Physical Science Basis. Contribution of Working Group I to the Fifth Assessment Report of the Intergovernmental Panel on Climate Change*, eds Stocker T, et al. (Cambridge Univ Press, New York), pp 159–254.
14. Holland M, Bitz C (2003) Polar amplification of climate change in coupled models. *Clim Dyn* 21(3-4):221–232.
15. Collins M, et al. (2013) Long-term climate change: Projections, commitments and irreversibility. *Climate Change 2013: The Physical Science Basis. Contribution of Working Group I to the Fifth Assessment Report of the Intergovernmental Panel on Climate Change*, eds Stocker T, et al. (Cambridge Univ Press, New York), pp 1029–1136.
16. Pithan F, Mauritsen T (2014) Arctic amplification dominated by temperature feedbacks in contemporary climate models. *Nat Geosci* 7(3):181–184.
17. Manabe S, Stouffer R (1980) Sensitivity of a global climate model to an increase of CO_2 concentration in the atmosphere. *J Geophys Res* 85(C10):5529–5554.
18. Winton M (2006) Amplified Arctic climate change: What does surface albedo feedback have to do with it? *Geophys Res Lett* 33(3):L03701.
19. Alexeev V, Langen P, Bates J (2005) Polar amplification of surface warming on an aquaplanet in "ghost forcing" experiments without sea ice feedbacks. *Clim Dyn* 24(7-8):655–666.
20. Manabe S, Stouffer R, Spelman M, Bryan K (1991) Transient responses of a coupled ocean-atmosphere model to gradual changes of atmospheric CO_2. Part I. Annual mean response. *J Clim* 4(8):785–818.
21. Graversen R, Langen P, Mauritsen T (2014) Polar amplification in CCSM4: Contributions from the lapse rate and surface albedo feedbacks. *J Clim* 27(12):4433–4450.
22. Curry J (1983) On the formation of continental polar air. *J Atmos Sci* 40(9):2278–2292.
23. Wexler H (1936) Cooling in the lower atmosphere and the structure of polar continental air. *Mon Weather Rev* 64(4):122–136.
24. Overland J, Guest P (1991) The Arctic snow and air temperature budget over sea ice during winter. *J Geophys Res* 96(C3):4651–4662.
25. Emanuel K (2008) Back to Norway: An essay. *Meteorol Monogr* 33(55):87–96.
26. Pithan F, Medeiros B, Mauritsen T (2014) Mixed-phase clouds cause climate model biases in Arctic wintertime temperature inversions. *Clim Dyn* 43(1-2):289–303.
27. Taylor K, Stouffer R, Meehl G (2012) An overview of CMIP5 and the experiment design. *Bull Am Meteorol Soc* 93(4):485–498.
28. Tsushima Y, et al. (2006) Importance of the mixed-phase cloud distribution in the control climate for assessing the response of clouds to carbon dioxide increase: A multi-model study. *Clim Dyn* 27(2-3):113–126.
29. Vavrus S, Waliser D, Schweiger A, Francis J (2009) Simulations of 20th and 21st century Arctic cloud amount in the global climate models assessed in the IPCC AR4. *Clim Dyn* 33(7-8):1099–1115.
30. Zelinka M, Klein S, Hartmann D (2012) Computing and partitioning cloud feedbacks using cloud property histograms. Part II: attribution to changes in cloud amount, altitude, and optical depth. *J Clim* 25(11):3736–3754.
31. Taylor P, et al. (2013) A decomposition of feedback contributions to polar warming amplification. *J Clim* 26(18):7023–7043.
32. Abbot D, Huber M, Bosquet G, Walker C (2009) High-CO_2 cloud radiative forcing feedback over both land and ocean in a global climate model. *Geophys Res Lett* 36(5): L05702.
33. Screen J (2014) Arctic amplification decreases temperature variance in northern mid- to high-latitudes. *Nat Clim Chang* 4(7):577–582.
34. Beesley J, Moritz R (1999) Toward an explanation of the annual cycle of cloudiness over the Arctic Ocean. *J Clim* 12(2):395–415.
35. Somerville R, Remer L (1984) Cloud optical thickness feedbacks in the CO_2 climate problem. *J Geophys Res* 89(D6):9668–9672.
36. Betts AK, Harshvardhan (1987) Thermodynamic constraint on the cloud liquid water feedback in climate models. *J Geophys Res* 92(D7):8483–8485.
37. Tselioudis G, Rossow W, Rind D (1992) Global patterns of cloud optical thickness variation with temperature. *J Clim* 5(12):1484–1495.
38. Eastman R, Warren S (2010) Interannual variations of Arctic cloud types in relation to sea ice. *J Clim* 23(15):4216–4232.
39. Liu Y, Key J, Liu Z, Wang X, Vavrus S (2012) A cloudier Arctic expected with diminishing sea ice. *Geophys Res Lett* 39(5):L05705.
40. Skamarock W, et al. (2008) A Description of the Advanced Research WRF Version 3 (Natl Cent Atmos Res, Boulder, CO).
41. Iacono M, et al. (2008) Radiative forcing by long-lived greenhouse gases: Calculations with the AER radiative transfer models. *J Geophys Res* 113(D13):D13103.
42. Hong S-Y, Noh Y, Dudhia J (2006) A new vertical diffusion package with explicit treatment of entrainment processes. *Mon Weather Rev* 134(9):2318–2341.
43. Kessler E (1969) *On the Distribution and Continuity of Water Substance in Atmospheric Circulations*, Meteorological Monographs (Am Meteorol Soc, Boston), Vol 32.
44. Lin Y-L, Farley R, Orville H (1983) Bulk parameterization of the snow field in a cloud model. *J Clim Appl Meteorol* 22(6):1065–1092.
45. Hong S-Y, Lim J-O (2006) The WRF single-moment 6-class microphysics scheme (WSM6). *J. Korean Meteorol. Soc.* 42(2):129–151.
46. Tao W-K, Simpson J, McCumber M (1989) An ice-water saturation adjustment. *Mon Weather Rev* 117(1):231–235.
47. Thompson G, Field P, Rasmussen R, Hall W (2008) Explicit forecasts of Winter precipitation using an improved bulk microphysics scheme. Part II: Implementation of a new snow parameterization. *Mon Weather Rev* 136(12):5095–5115.
48. Morrison H, Thompson G, Tatarskii V (2009) Impact of cloud microphysics on the development of trailing stratiform precipitation in a simulated squall line: Comparison of one- and two-moment schemes. *Mon Weather Rev* 137(3):991–1007.
49. Lin Y, Colle B (2011) A new bulk microphysical scheme that includes riming intensity and temperature-dependent ice characteristics. *Mon Weather Rev* 139(3):1013–1035.

Supporting Information

Cronin and Tziperman 10.1073/pnas.1510937112

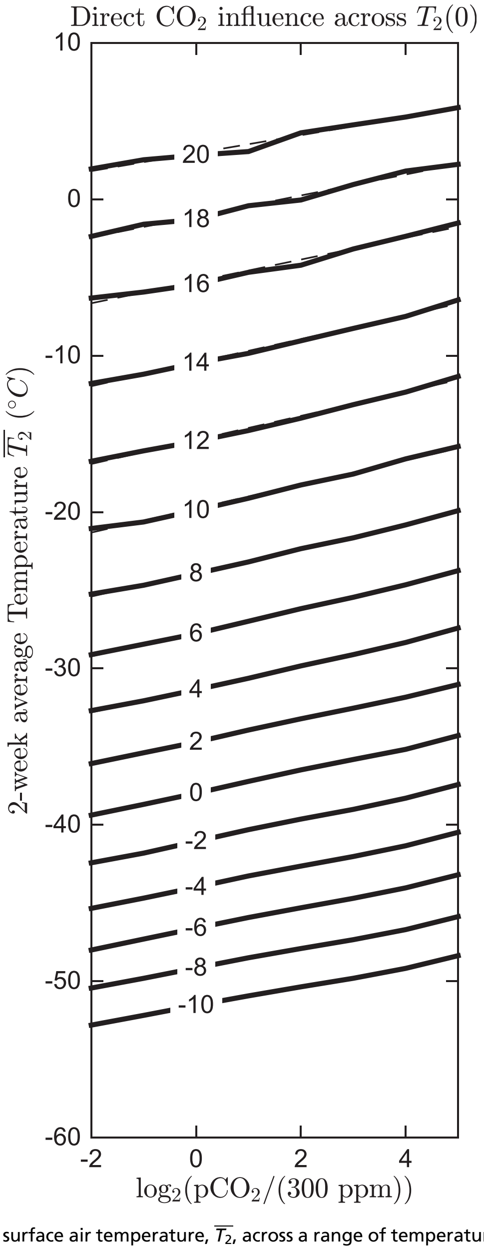

Fig. S1. Direct influence of pCO_2 on 2-wk average surface air temperature, $\overline{T_2}$, across a range of temperatures. Note the logarithmic horizontal axis; minimum pCO_2 is 75 ppm, and maximum is 9,600 ppm. Solid black lines indicate mean across microphysics schemes, numbers on each line indicate the initial 2-m air temperature $T_2(0)$, and dashed black lines indicate fits $\overline{T_2} = m\log_2(pCO_2) + b$. Slopes m vary from 0.57 °C to 0.77 °C per doubling of pCO_2.

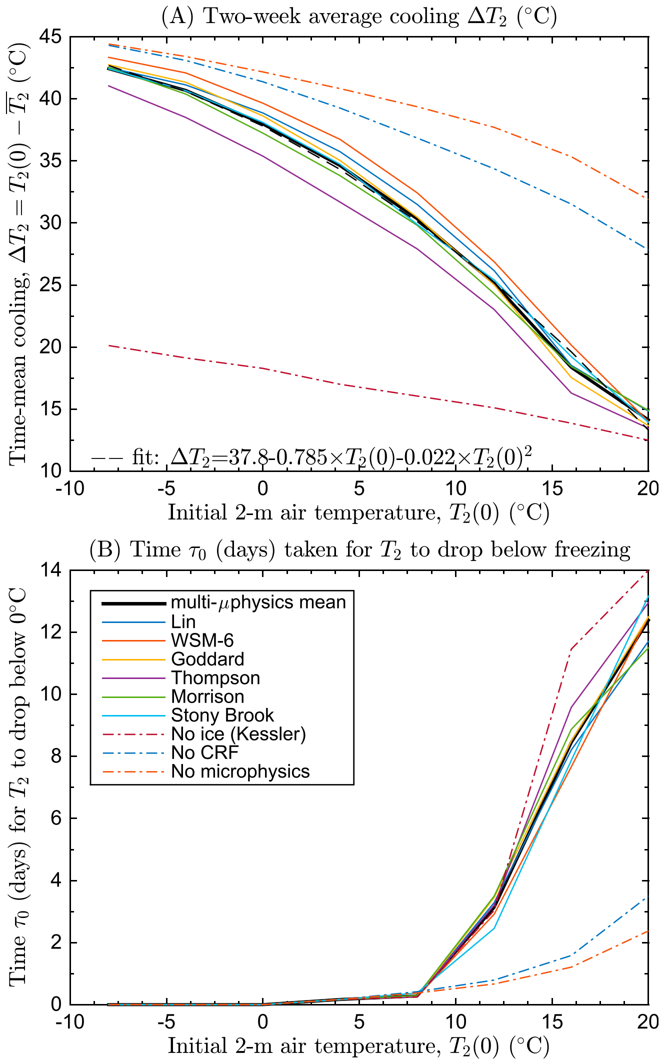

Fig. S2. As in Fig. 2, but with pCO_2 doubled for each 4 °C increase in $T_2(0)$; pCO_2 = (75, 150, 300, 600, 1,200, 2,400, 4,800, 9,600) ppm for $T_2(0)$ = (−8, −4, 0, 4, 8, 12, 16, 20) °C, respectively. Results are similar to those without CO_2 changes (Fig. 2), and principal differences from the results in Fig. 2 include more cooling at low $T_2(0)$, less cooling at high $T_2(0)$, and an increase in the magnitude of the slopes of the "no microphysics" and "no CRF" dash-dotted lines, which both use only clear-sky radiative transfer.

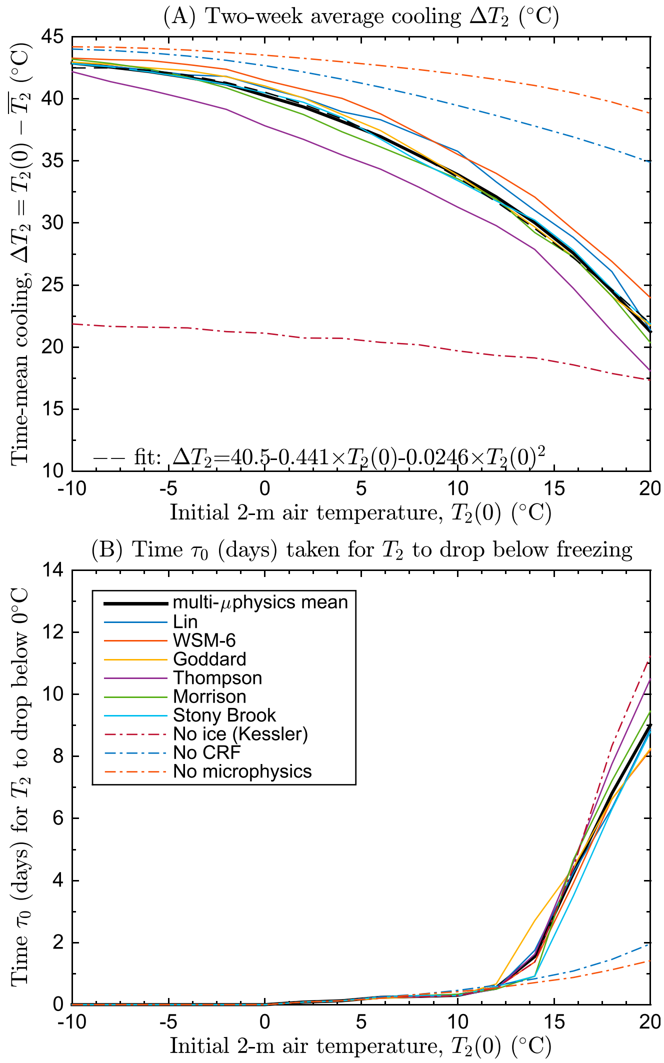

Fig. S3. As in Fig. 2, but with a drier initial sounding, having 70% relative humidity at the surface, decreasing to 10% relative humidity at 600 hPa and above to the tropopause. Principal differences from results in Fig. 2 include more cooling, especially at high $T_2(0)$, and consequently smaller sensitivity of ΔT_2 to $T_2(0)$.

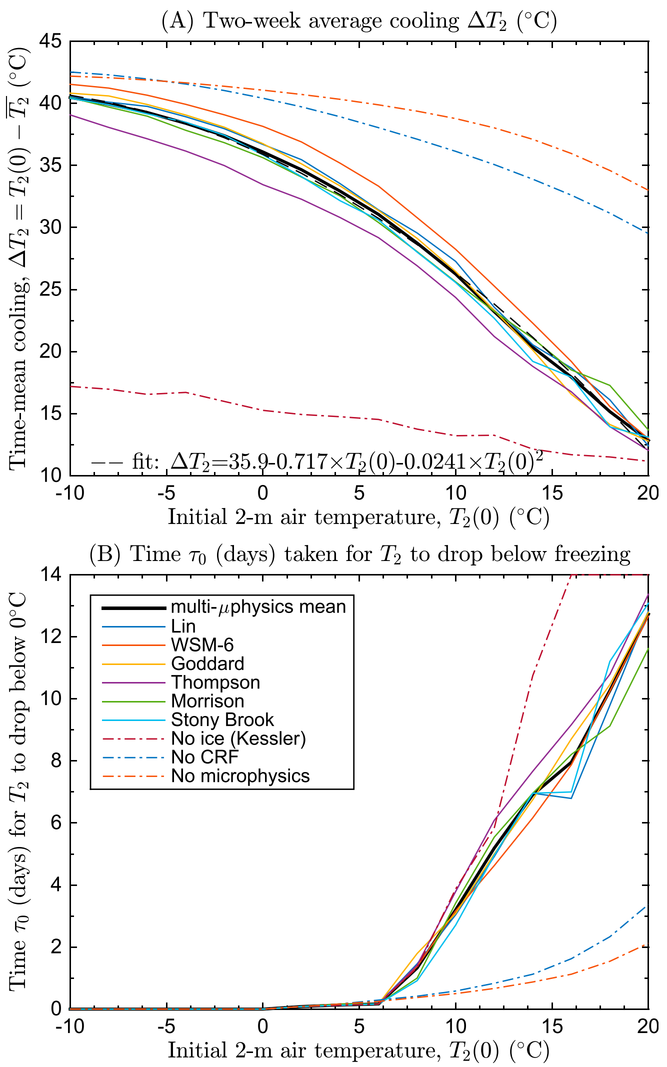

Fig. S4. As in Fig. 2, but with a moister initial sounding, having 90% relative humidity at the surface, decreasing to 30% relative humidity at 600 hPa and above to the tropopause. Principal differences from results in Fig. 2 include less cooling, especially at high $T_2(0)$, and consequently larger sensitivity of ΔT_2 to $T_2(0)$.

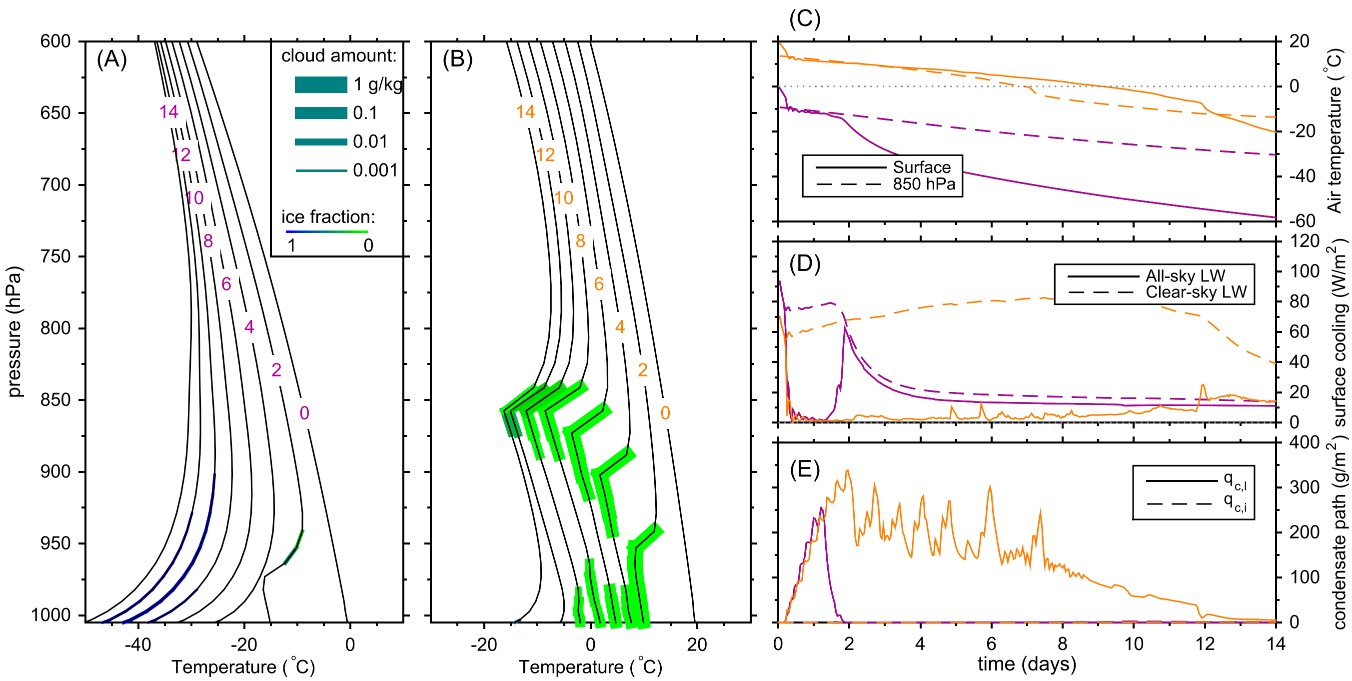

Fig. S5. As in Fig. 1, but with an imposed subsidence profile, with subsidence peaking at 2 mm/s at z = 4 km, and decreasing to zero for z = 0 km and z = 12 km; the expression for $w(z)$ is given in *Materials and Methods*. Principal differences from results in Fig. 1 include more cooling in the lowest 100–150 hPa of the troposphere, a sharper cloud-top inversion for the warmer initial condition, and less cooling aloft.

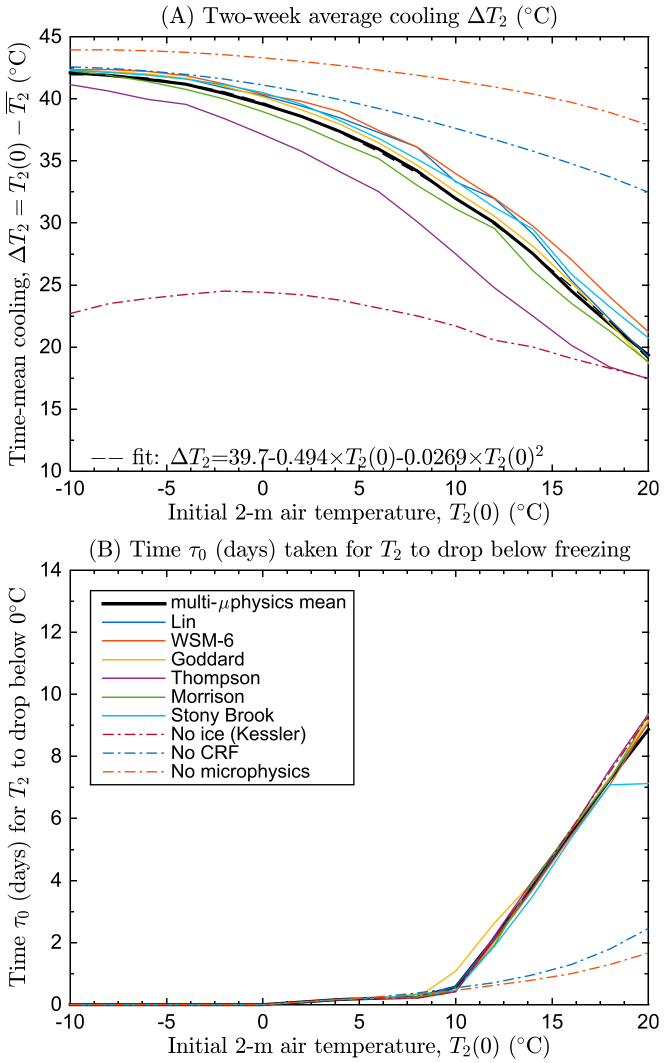

Fig. S6. As in Fig. 2, but with an imposed subsidence profile, as described in Fig. S5 and in *Materials and Methods*. Principal differences from results in Fig. 2 include slightly more cooling, reduced sensitivity of ΔT_2 to $T_2(0)$, and shorter times taken for the surface to reach freezing.

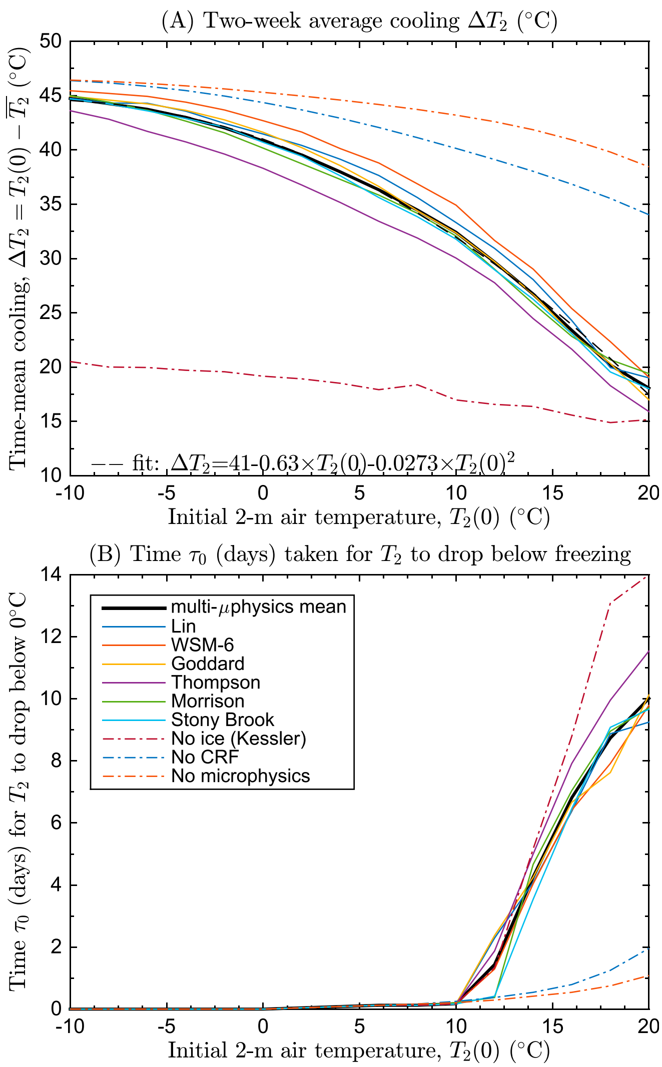

Fig. S7. As in Fig. 2, but with a smaller thickness of the ground layer, $z_{eff} = 2$ cm instead of $z_{eff} = 5$ cm. Principal differences from results in Fig. 2 include more cooling, especially at low $T_2(0)$, and consequently larger sensitivity of ΔT_2 to $T_2(0)$. Note the expanded vertical scale in *A*, compared with Fig. 2.

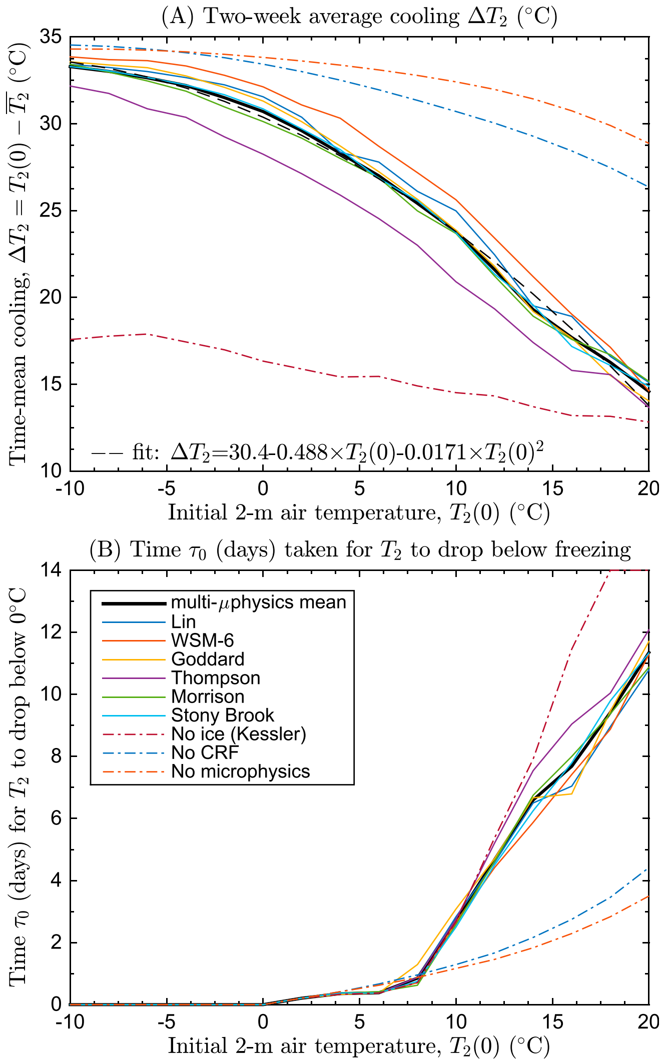

Fig. S8. As in Fig. 2, but with a larger thickness of the ground layer, $z_{eff} = 15$ cm instead of $z_{eff} = 5$ cm. Principal differences from results in Fig. 2 include less cooling, especially at low $T_2(0)$, and consequently smaller sensitivity of ΔT_2 to $T_2(0)$. Note the contracted vertical scale in *A*, compared with Fig. 2.

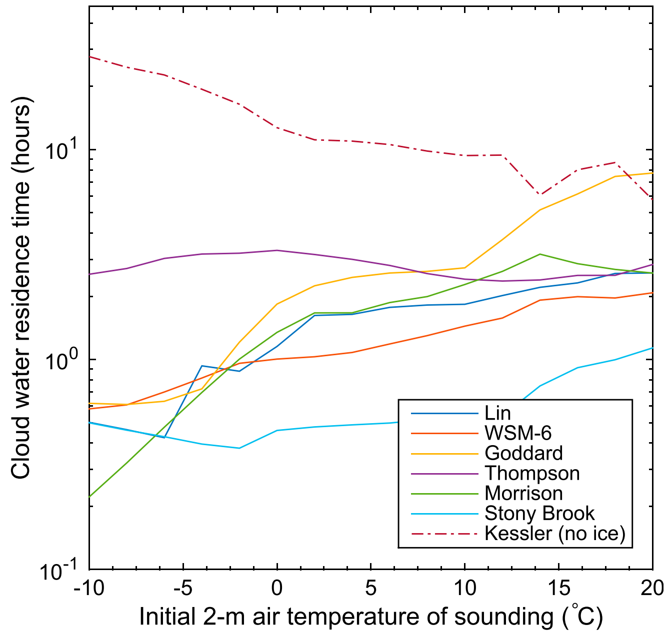

Fig. S9. Cloud water residence time plotted against initial 2-m air temperature $T_2(0)$ for each of the microphysics schemes in Fig. 2. Cloud water residence time is defined as the time mean vertically integrated cloud condensate (in kilograms per square meter), divided by the time mean surface precipitation rate (in kilograms per square meter per second). Note the logarithmic vertical axis; straight lines thus correspond to exponentially increasing or decreasing time scales with temperature; a factor of 10 change across the 30-degree temperature range shown here corresponds to $\sim$ 7.5% per degree Celsius. Most microphysics schemes show an increase in cloud water residence time with temperature, although the increase is not always monotonic (e.g., Stony Brook), and one scheme does not show an average increase in cloud water residence time with temperature (Thompson).